

Global lake evaporation accelerated by changes in surface energy allocation in a warmer climate

Wei Wang^{1,2,5}, Xuhui Lee^{1,3*}, Wei Xiao^{1,2,5}, Shoudong Liu^{1,2}, Natalie Schultz³, Yongwei Wang^{1,2}, Mi Zhang^{1,2} and Lei Zhao^{1,4}

Lake evaporation is a sensitive indicator of the hydrological response to climate change. Variability in annual lake evaporation has been assumed to be controlled primarily by the incoming surface solar radiation. Here we report simulations with a numerical model of lake surface fluxes, with input data based on a high-emissions climate change scenario (Representative Concentration Pathway 8.5). In our simulations, the global annual lake evaporation increases by 16% by the end of the century, despite little change in incoming solar radiation at the surface. We attribute about half of this projected increase to two effects: periods of ice cover are shorter in a warmer climate and the ratio of sensible to latent heat flux decreases, thus channelling more energy into evaporation. At low latitudes, annual lake evaporation is further enhanced because the lake surface warms more slowly than the air, leading to more long-wave radiation energy available for evaporation. We suggest that an analogous change in the ratio of sensible to latent heat fluxes in the open ocean can help to explain some of the spread among climate models in terms of their sensitivity of precipitation to warming. We conclude that an accurate prediction of the energy balance at the Earth's surface is crucial for evaluating the hydrological response to climate change.

In the climate system, lakes represent wet surfaces at which evaporation is controlled only by atmospheric conditions^{1,2} and is therefore highly sensitive to climate change³. Current understanding of the influence of climate variability on annual lake evaporation E is that E is primarily limited by incoming surface solar radiation⁴ (K_1), a view supported by the close relationship between pan evaporation trends and the dimming and brightening cycles of K_1 (refs^{5,6}). However, because of their negligible thermal inertia and the lack of ice phenology, evaporation pans are not ideal proxies for lake systems.

About 85% of the 250,000 lakes in the world are located at mid- to high latitudes⁷ (north of 40°N or south of 40°S) where the water remains frozen for some part of the year. As the temperature rises, the lake will freeze later in the winter and thaw sooner in the spring⁸. The shortened ice period will result in a higher absorption of K_1 because open water has a much lower albedo (a) than ice. During the open water season, lake evaporation occurs at a potential rate constrained by the surface radiation energy. According to the Priestley–Taylor (PT) model of potential evaporation⁹, the lake Bowen ratio (β) will be reduced in a warmer climate, the consequence being that more energy is allocated to support evaporation. Both reduced a and β will cause E to increase (Fig. 1). The adjustment of the lake surface temperature to these changes in energy allocation constitutes a feedback mechanism that can either further enhance E or damp its rise. Owing to the faster evaporation rate, the surface of low-latitude lakes is expected to warm more slowly than the overlying air, leading to a smaller outgoing long-wave radiation loss and therefore more net long-wave radiation energy available for evaporation. On the other hand, increased absorption of K_1 by high-latitude lakes should cause faster warming of the lake surface, and the resulting higher surface long-wave radiation loss represents

a negative feedback on E . These mechanisms are fundamentally different from those involved in pan evaporation.

Here we hypothesize that the changes in surface energy allocation are a key driver of the response of lake E to rising temperatures. We test this hypothesis using a lake simulator forced with the Representative Concentration Pathway (RCP) 8.5 climate warming scenario in an Earth system model¹⁰. The lake simulator, which has realistic representation of surface fluxes, snow and ice phenology, and sediment heat exchange, has been extensively tested against field observations¹¹. Our own evaluation of its lake E calculation also reveals excellent performance (Supplementary Fig. 1). In the model, the lake–atmosphere interactions occur at the subgrid scale¹² and the global lake distribution (size and depth) is prescribed according to the Global Lake and Wetland Database^{7,13}. The simulation is done at hourly intervals from 2005 to 2100 after 120 years of spin-up. The subgrid outputs are then used in an offline diagnostic analysis of the surface energy balance^{5,14} to isolate the contributions of various mechanisms to the modelled E changes. We focus on absolute changes between the last (2091–2100) and the first 10 years (2006–2015) of the simulation, with Δ denoting the change. For example, $\Delta(\lambda E)$ is the lake latent heat flux difference between these two periods (mean of last period minus mean of first period). Unless stated otherwise, all quantities are mean values weighted by lake area.

Contributions to lake evaporation change

In spite of a negligible change in K_1 ($\Delta K_1 = -0.6 \text{ W m}^{-2}$), the lake E shows a universal increasing pattern across the world (Fig. 2). The largest ΔE , about 210 mm y^{-1} (or $\Delta(\lambda E)$ of 16.5 W m^{-2}) occurs at low latitudes (30°S to 30°N), but because 60% of the global lake area is found at higher latitudes⁷, the global mean change is smaller (ΔE of 140 mm y^{-1} , or $\Delta(\lambda E)$ of 11.1 W m^{-2} ; Fig. 3a), which

¹Yale–NUIST Center on Atmospheric Environment, International Joint Laboratory on Climate and Environment Change, Nanjing University of Information Science & Technology, Nanjing, China. ²Key Laboratory of Meteorological Disaster, Ministry of Education & Collaborative Innovation Center on Forecast and Evaluation of Meteorological Disasters, Nanjing University of Information Science & Technology, Nanjing, China. ³School of Forestry and Environmental Studies, Yale University, New Haven, CT, USA. ⁴Program in Science, Technology, and Environmental Policy, Woodrow Wilson School of Public and International Affairs, Princeton University, Princeton, NJ, USA. ⁵These authors contributed equally: Wei Wang and Wei Xiao. *e-mail: xuhui.lee@yale.edu

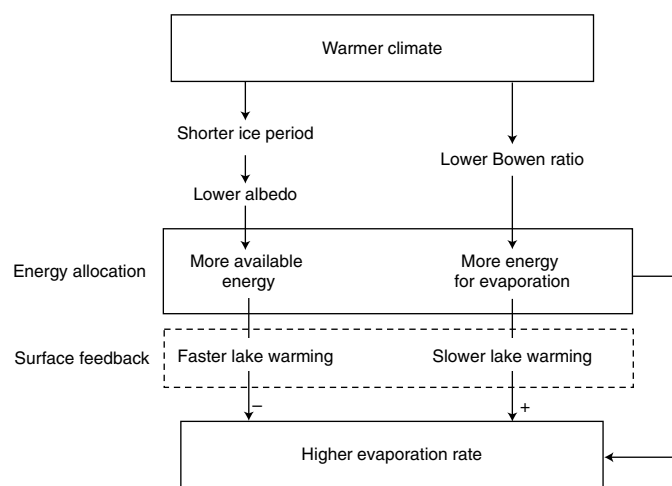


Fig. 1 | Conceptual diagram of lake evaporation changes in a warmer climate. Lake evaporation trends are influenced by both energy allocation through changes in Bowen ratio and albedo and surface radiative feedback through surface temperature adjustment.

corresponds to a relative increase of 16%. The global lake mean α and β are reduced from 0.134 and 0.088 in 2006–2015 to 0.114 and 0.064 in 2091–2100, respectively. These changes in surface energy allocation contribute 4.7 W m^{-2} , or about half of the total $\Delta(\lambda E)$. The rest of the λE increase results from changes in atmospheric forcing and surface feedback (4.3 W m^{-2}) and from change in snowmelt energy (1.9 W m^{-2}).

The reduction in α is the result of shortened ice periods at mid- to high latitudes. Our model calculation reveals an albedo temperature sensitivity of -0.0046 K^{-1} or a relative decrease of $3.4\% \text{ K}^{-1}$ (global mean). The response of β to temperature is more complex, but a predictive understanding is provided by the PT model of open-water evaporation. According to the model, β is a convex function of temperature, decreasing from about 1.0 at 0°C to 0.08 at 25°C . The model also predicts lower values of β for lakes at higher altitudes because the psychrometric constant is proportional to pressure. These patterns are broadly consistent with observational data and the lake simulator results (Fig. 4a). The high bias of the PT β values between 10 and 20°C suggests that the non-equilibrium effect may

be stronger than assumed by the PT model. Forcing good agreement with the lake simulator requires that the PT model parameter (α) be changed from the original value of 1.26 to about 1.31. This updated α value matches very well with that derived from the ocean latent and sensible heat fluxes observed under the current climate conditions¹⁵. The modelled β values for the first and last 10 years of the simulation essentially follow the same PT model prediction (Supplementary Fig. 6), suggesting that the effect of energy advection on lake E is insensitive to climate change. Both the PT model and the lake simulator predict a larger β temperature sensitivity for lakes in colder climates (Fig. 4b). But because the change in lake E is proportional to the relative change in β (that is, $\Delta\beta/\beta$) and β is small at low latitudes, changes in latent and sensible heat partitioning contribute more to $\Delta(\lambda E)$ in the tropical climate than in the cold climate (Fig. 3b,e).

Another regional difference is explained by snowmelt. At present, 9.0 and 17.5 W m^{-2} of the surface radiation energy are consumed by spring snowmelt in the cold and polar climate regions, respectively. At the end of the century, these numbers are projected to be 5.9 and 13.9 W m^{-2} due to reductions in snowfall. Reduced snowmelt is the second largest contributor (second only to α reduction) to the lake E increase in these climatic regions (Fig. 3e,f). The phase changes of water also modify energy allocation, but their effect is to move energy from the surface (by consuming latent heat via evaporation and snowmelt) to the lower atmosphere (by releasing latent heat via cloud condensation and freezing¹⁵). Our results show that the expected shift to more liquid precipitation in a warmer climate¹⁶ will increase lake evaporation (Fig. 3e,f). More generally, the shift in precipitation form constitutes a weakened latent heat exchange between the land and the atmosphere, which should amplify the warming of the land surface at mid- to high latitudes, although the extent of this snowmelt effect on surface temperature is not known.

Lake surface temperature adjustment

The lake surface temperature adjustment follows a bimodal pattern (Supplementary Fig. 2a). The surface temperature T_s of current ice-free lakes at low latitudes rises more slowly than the air temperature T_a , in agreement with previous lake modelling studies^{17,18}, whereas T_s of high-latitude lakes (with current ice periods exceeding 65 days per year) increases at the same pace as T_a . Satellite data suggest that low- and high-latitude lakes respond to warming differently^{19,20}. At low latitudes, the slow T_s adjustment is well explained by the reduction in β (Supplementary Fig. 2b) according to the intrinsic

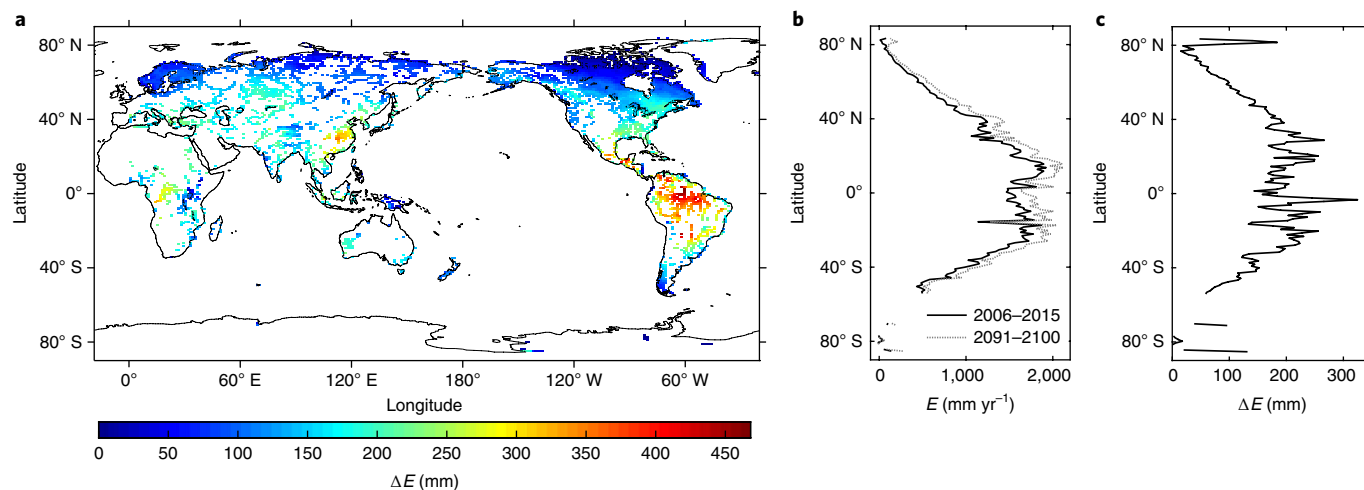


Fig. 2 | Changes in annual lake evaporation. **a**, Spatial distribution of ΔE (2091–2100 mean minus 2006–2015 mean). **b**, Zonal mean of lake evaporation in the first 10 years (2006–2015) and the last 10 years (2091–2100). **c**, Zonal mean of lake evaporation change.

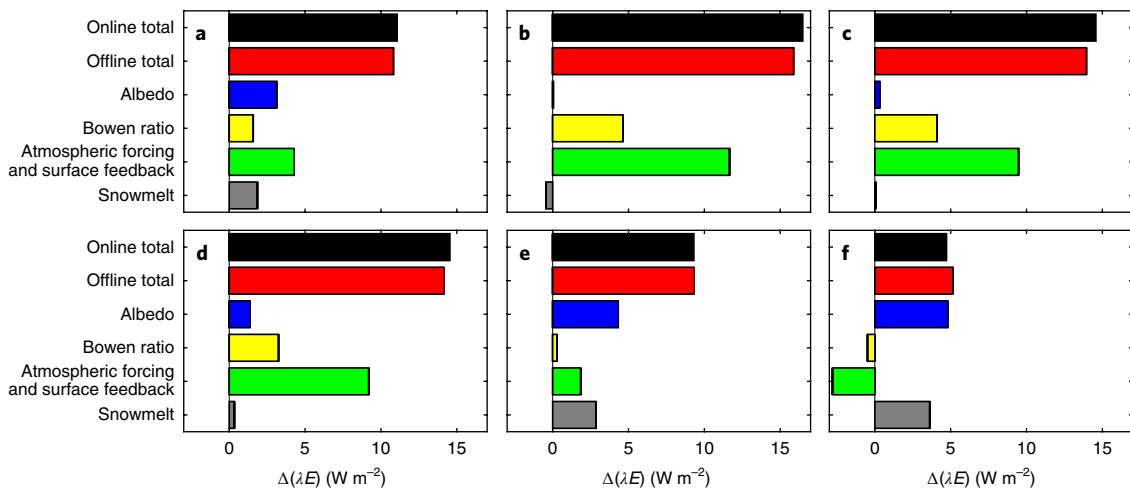


Fig. 3 | Attribution of lake latent heat flux change. **a**, Global change in latent heat flux. **b–f**, Change in latent heat flux for tropical (**b**), temperate (**c**), arid (**d**), cold (**e**) and polar (**f**) climates. Black bars show $\Delta(\lambda E)$ between 2091–2100 and 2006–2015 predicted by online model calculation; red bars show $\Delta(\lambda E)$ calculated as the sum of the four component contributions, blue bars indicate the contribution of albedo change, yellow bars show the contribution of β change, green bars show the contributions of the changes in atmospheric forcing and surface feedback, grey bars show the contribution of changes in snowmelt energy.

biophysical theory of surface energy allocation¹⁴ and is consistent with experimental evidence provided by a long-term field observation²¹. The ΔT_s of these lakes is on average 0.6°C lower than ΔT_a . Consequently, these lakes lose 3.0 W m^{-2} less long-wave radiation energy than if T_s were to increase at the same rate as T_a . For comparison, ΔL_i , the change in the incoming long-wave radiation due to greenhouse gas buildup in the atmosphere, is 25.6 W m^{-2} , and the net long-wave radiation change ΔL_n is 5.2 W m^{-2} . The slow T_s adjustment is essentially a positive feedback that amplifies the response of lake E to warming (Supplementary Fig. 3b,c).

Comparison with land and ocean evaporation

The results presented here are probably the upper bound of the hydrological response to climate warming. Terrestrial E falls between water-limited and energy-limited regimes²². While lakes are energy-limited systems, most upland ecosystems are water-limited. Globally, about 80% of the historical variation in terrestrial

E is constrained by soil moisture limitation for at least some part of the year²³. Although soil moisture may be less limiting due to increases in precipitation in the future, terrestrial E is expected to be reduced by stomatal downregulation by 1–4 % for doubling of the atmospheric CO_2 ^{24,25} and by up to 8% under RCP8.5²⁶.

Although the relative change in the global lake E (16%) is similar to the projected increase in atmospheric water vapour content²⁷, oceanic E is much less sensitive to temperature increases²⁸. This low sensitivity can also be understood via the framework of the surface energy balance. One cause of the muted sensitivity is a much smaller fraction of seasonal ice cover in the oceans than in the lakes, and hence a negligible ice albedo effect on ocean E . Changes in energy allocation via β are still a large contributor to the increase in E (Supplementary Fig. 4), but the oceanic β temperature sensitivity is smaller in magnitude than the PT model prediction (Supplementary Fig. 5), implying a shift of ocean E towards the equilibrium E in the future. Finally, the ocean surface temperature

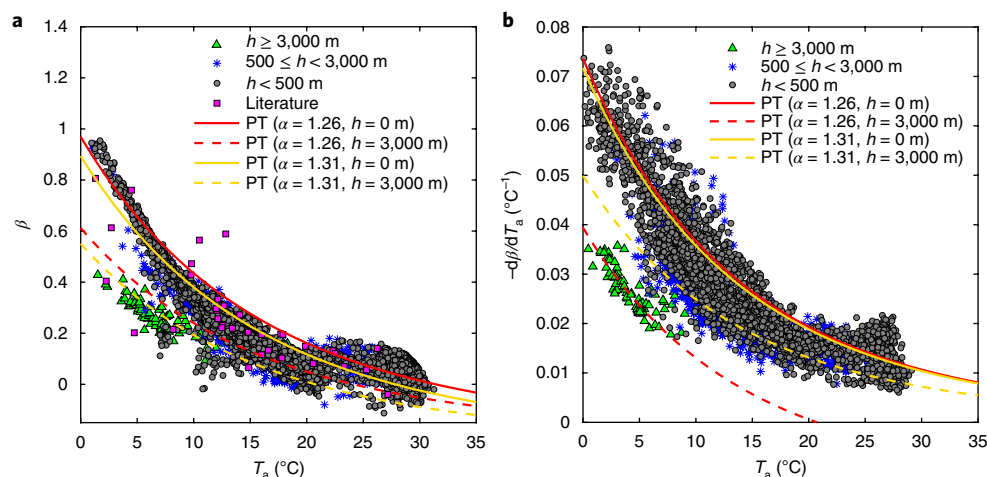


Fig. 4 | Temperature controls on lake Bowen ratio. **a**, β as a function of T_a . Each data point represents the mean of 2005–2100 for one lake. **b**, Temperature sensitivity of β . Each data point represents the sensitivity of one lake obtained by linear regression of the lake β against temperature over the period 2005–2100. Lake E data found in the literature and the PT model prediction with two different parameter value ($\alpha = 1.26$ and 1.31) are also shown. Lake altitude is denoted by h .

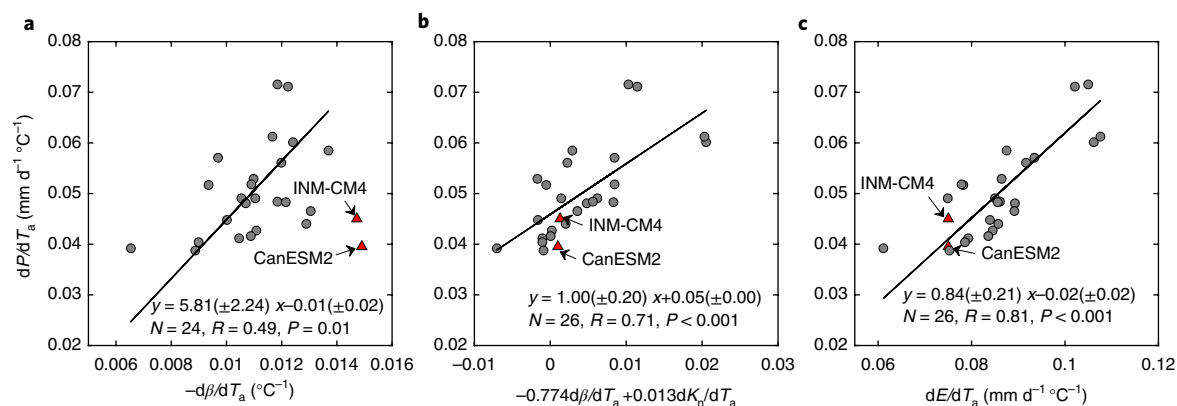


Fig. 5 | Global precipitation temperature sensitivity in CMIP5 models. **a**, Global precipitation (P) temperature sensitivity versus β temperature sensitivity. **b**, Global P temperature sensitivity versus a composite index $-0.774d\beta/dT_a + 0.013dK_s/dT_a$, where dK_s/dT_a is temperature sensitivity of surface net shortwave radiation. **c**, Global P temperature sensitivity versus ocean E temperature sensitivity. The solid lines represent linear regressions with the regression statistics noted (N , number of models; R , linear correlation coefficient). Two outliers, marked by red filled triangle with model names noted, are excluded from the statistics shown in **a**.

increases at the same rate according to historical data²⁹ and at nearly the same rate as the oceanic air temperature according to climate model projections ($\Delta T_s - \Delta T_a = -0.07 \pm 0.06$ °C, mean ± 1 s.d. of 26 Coupled Model Intercomparison Project Phase 5 (CMIP5) models³⁰). In other words, the positive feedback via slow T_s adjustment expected of low-latitude lakes does not apply to ocean E .

Global precipitation temperature sensitivity

In summary, our energy balance analysis supports the hypothesis that changes in surface energy allocation play important roles in future changes of global lake E . The same energy balance considerations also offer strong constraints on the water flux of the open oceans to the atmosphere, the main source of water vapour for sustaining global precipitation. A roadblock that confronts the climate modelling community is the large variation in precipitation temperature sensitivity among global climate models, the explanation for which has remained elusive so far²⁷. We find that the global precipitation temperature sensitivity is highly correlated with the oceanic β temperature sensitivity among the CMIP5 models ($P < 0.05$; Fig. 5a), and that the β sensitivity together with the temperature sensitivity of the surface shortwave radiation explains nearly 50% of the spread in the precipitation sensitivity among these models ($P < 0.001$; Fig. 5b). Generally, models that show modest changes in K_s and β also predict weak increase in global precipitation towards the end of the century. The climate modelling community has been paying a great deal of attention to the energy balance at the top of the atmosphere as a way of quantifying climate feedbacks. Our study suggests that, in terms of the hydrological response to climate change, what matters the most is accurate prediction of the energy balance at the Earth's surface.

Methods

Methods, including statements of data availability and any associated accession codes and references, are available at <https://doi.org/10.1038/s41561-018-0114-8>.

Received: 1 February 2018; Accepted: 27 March 2018;
Published online: 30 April 2018

References

- Brutsaert, W. & Parlange, M. B. Hydrologic cycle explains the evaporation paradox. *Nature* **396**, 30 (1998).
- McMahon, T. A. et al. Estimating actual, potential, reference crop and pan evaporation using standard meteorological data: a pragmatic synthesis. *Hydrol. Earth Syst. Sci.* **17**, 1331–1363 (2013).

- Adrian, R. et al. Lakes as sentinels of climate change. *Limnol. Oceanogr.* **54**, 2283–2297 (2009).
- Linacre, E. T. Evaporation trends. *Theor. Appl. Climatol.* **79**, 11–21 (2004).
- Roderick, M. L. & Farquhar, G. D. The cause of decreased pan evaporation over the past 50 years. *Science* **298**, 1410–1411 (2002).
- Wild, M. et al. From dimming to brightening: decadal changes in solar radiation at earth's surface. *Science* **308**, 847–850 (2005).
- Lehner, B. & Döll, P. Development and validation of a global database of lakes, reservoirs and wetlands. *J. Hydrol.* **296**, 1–22 (2004).
- Magnuson, J. J. et al. Historical trends in lake and river ice cover in the northern hemisphere. *Science* **289**, 1743–1746 (2000).
- Priestley, C. H. B. & Taylor, R. J. On the assessment of surface heat flux and evaporation using large-scale parameters. *Mon. Weather Rev.* **100**, 81–92 (1972).
- Hurrell, J. W. et al. The Community Earth System Model: a framework for collaborative research. *Bull. Am. Meteorol. Soc.* **94**, 1339–1360 (2013).
- Subin, Z. M., Riley, W. J. & Mironov, D. An improved lake model for climate simulations: model structure, evaluation, and sensitivity analyses in CESM1. *J. Adv. Model. Earth Syst.* **4**, M02001 (2012).
- Oleson, K. et al. *Technical Description of Version 4.5 of the Community Land Model (CLM)* Technical Note NCAR/TN-503+STR (NCAR, 2013).
- Kourzeneva, E. et al. Global gridded dataset of lake coverage and lake depth for use in numerical weather prediction and climate modelling. *Tellus A* **64**, 15640 (2012).
- Lee, X. et al. Observed increase in local cooling effect of deforestation at higher latitudes. *Nature* **479**, 384–387 (2011).
- Trenberth, K. E., Fasullo, J. T. & Kiehl, J. Earth's global energy budget. *Bull. Am. Meteorol. Soc.* **90**, 311–323 (2009).
- Wentz, F. J. et al. How much more rain will global warming bring? *Science* **317**, 233–235 (2007).
- Schmid, M., Hunziker, S. & Wüest, A. Lake surface temperatures in a changing climate: a global sensitivity analysis. *Climatic Change* **124**, 301–315 (2014).
- Butcher, J. B. et al. Sensitivity of lake thermal and mixing dynamics to climate change. *Climatic Change* **129**, 295–305 (2015).
- Schneider, P. & Hook, S. J. Space observations of inland water bodies show rapid surface warming since 1985. *Geophys. Res. Lett.* **37**, L22405 (2010).
- O'Reilly, C. M. et al. Rapid and highly variable warming of lake surface waters around the globe. *Geophys. Res. Lett.* **42**, 10773–10781 (2015).
- Lenters, J. D., Kratz, T. K. & Bowser, C. J. Effects of climate variability on lake evaporation: Results from a long-term energy budget study of Sparkling Lake, northern Wisconsin (USA). *J. Hydrol.* **308**, 168–195 (2005).
- Wang, K. & Dickinson, R. E. A review of global terrestrial evapotranspiration: observation, modeling, climatology, and climatic variability. *Rev. Geophys.* **50**, RBG2005 (2012).
- Jung, M. et al. Recent decline in the global land evapotranspiration trend due to limited moisture supply. *Nature* **467**, 951–954 (2010).
- Betts, R. A. et al. Projected increase in continental runoff due to plant responses to increasing carbon dioxide. *Nature* **448**, 1037–1042 (2007).

25. Swann, A. L. S. et al. Plant responses to increasing CO₂ reduce estimates of climate impacts on drought severity. *Proc. Natl Acad. Sci. USA* **113**, 10019–10024 (2016).
26. Skinner, C. B. et al. The role of plant CO₂ physiological forcing in shaping future daily-scale precipitation. *J. Clim.* **30**, 2319–2340 (2017).
27. Collins, M. et al. in *Climate Change 2013: The Physical Science Basis* (eds Stocker, T. F. et al.) Ch. 12 (IPCC, Cambridge Univ. Press, 2013).
28. Schneider, T., O’Gorman, P. A. & Levine, X. J. Water vapor and the dynamics of climate changes. *Rev. Geophys.* **48**, RG3001 (2010).
29. Trenberth, K. E. et al. in *Climate Change 2007: The Physical Science Basis* (eds Solomon, S. et al.) Ch. 3 (IPCC, Cambridge Univ. Press, 2007).
30. Taylor, K. E., Stouffer, R. J. & Meehl, G. A. An overview of CMIP5 and the experiment design. *Bull. Am. Meteorol. Soc.* **93**, 485–498 (2012).

Acknowledgements

This research was supported by the National Natural Science Foundation of China (grant nos 41505005, 41475141, 41575147 and 41275024), the Natural Science Foundation of Jiangsu Province, China (grant no. BK20150900), the Ministry of Education of China (grant PCSIRT) and the Priority Academic Program Development of Jiangsu Higher Education Institutions (grant PAPD). We thank Z. Zubin for running the historical lake simulation. The futuristic simulation was supported by

high-performance computing from Yellowstone (ark:/85065/d7wd3xhc) provided by NCAR’s Computational and Information Systems Laboratory, sponsored by the US National Science Foundation.

Author contributions

X.L. designed the research, L.Z. performed the model simulation and W.W. carried out the analysis. S.L., N.S., W.X., Y.W. and M.Z. contributed ideas to the data analysis and manuscript writing, and X.L. and W.W. wrote the manuscript.

Competing interests

The authors declare no competing interests.

Additional information

Supplementary information is available for this paper at <https://doi.org/10.1038/s41561-018-0114-8>.

Reprints and permissions information is available at www.nature.com/reprints.

Correspondence and requests for materials should be addressed to X.L.

Publisher’s note: Springer Nature remains neutral with regard to jurisdictional claims in published maps and institutional affiliations.

Methods

The lake simulator. The lake simulator is part of the Community Land Model (CLM, version 4.5), which uses a nested hierarchy consisting of up to five land units or tiles (glacier, urban, agricultural, vegetation and lake) to represent the land surface heterogeneity at the subgrid level¹². It explicitly considers heat diffusion in snow, ice, water, sediment and bedrock layers¹¹. Heat diffusion in the water column includes the Henderson–Sellers formulation for eddy diffusion³¹, wind-driven mixing³², buoyant convection, mixing by three-dimensional circulations³³ and molecular conduction. The heat, moisture and momentum fluxes between the lake water surface and the overlying atmosphere are calculated with the bulk transfer approach. Ice and snow phenology are parameterized similarly to the phase-change solutions for other land tiles in CLM³⁴. Within the CLM hierarchy, the lake simulator calculates the surface fluxes of the lake tile at the subgrid level. The lake areal fraction and lake depth are prescribed according to the Global Lake and Wetland Database⁷ and the global gridded dataset of lake coverage and lake depth designed for numerical weather prediction and climate modelling¹³.

Two lake simulations, namely historical and future, were run at a high horizontal resolution (grid size: 0.94° latitude × 1.25° longitude). The historical simulation was performed using the 1991–2010 CRUNCEP atmospheric forcing data for 81 years, with the first 61 years devoted to spin-up. The calculated annual evaporation flux was compared with lake evaporation data found in the literature, using the years and the grid points where such data exist, to evaluate the model performance (Supplementary Fig. 1; Supplementary Table 1). The future simulation was driven by the 2005–2100 atmospheric outputs from the fully coupled run of the Community Earth System Model (CESM)¹⁰ under the RCP 8.5 scenario after a spin-up of 120 years. The driving atmospheric outputs were generated using the same version of CLM imbedded in CESM, ensuring consistency. This approach is basically a retrieval of the surface variables from the fully coupled CESM run, producing nearly identical outputs to those obtained from the online simulation³⁵. The subgrid variables pertaining to the surface energy balance of the lake tile were used in the offline diagnostic analysis of the spatiotemporal variations in global lake evaporation and their driving factors.

Offline diagnostic analysis of the surface energy balance. We used a surface energy balance analysis to isolate the contributions of forcing variables, energy allocation and surface feedback to the model-predicted $\Delta(\lambda E)$ using an approach similar to those adopted by earlier studies^{5,14,36}. According to the surface energy balance principle, the lake latent heat flux λE is given by

$$\lambda E = \frac{(1-a)K_1 + L_1 - L_1 - G}{1 + \beta} \quad (1)$$

where L_1 and L_1 are incoming and outgoing long-wave radiation, respectively, and G is heat storage term. The annual mean G is zero for lakes at low latitudes and is positive at mid- to high latitudes due to energy consumption by snowmelt.

Differentiating equation (1), we obtain,

$$\Delta(\lambda E) = -\frac{R_n - G}{(1 + \beta)^2} \Delta\beta - \frac{K_1}{1 + \beta} \Delta a + \frac{1}{1 + \beta} [(1-a)\Delta K_1 + \Delta L_1 - \Delta L_1] - \frac{1}{1 + \beta} \Delta G \quad (2)$$

where $R_n = (1-a)K_1 + L_1 - L_1$ is the surface net radiation and Δ denotes change between the last (2091–2100) and the first 10 years (2006–2015) of the model run. The first, second, third and fourth term on the right-hand side of equation (2) represent contributions from changes in the Bowen ratio or energy partitioning, the lake surface albedo, atmospheric forcing and long-wave feedback, and snowmelt energy, respectively. This diagnostic analysis is applied at the global scale as well as to five climate zones (tropical: 17% lake area; temperate: 12%; arid: 7%; cold: 54%; polar: 10%) according to the Köppen–Geiger climate classification³⁷. For convenience of presentation, Fig. 2 gives the sum of the contributions from changes in atmospheric forcing (ΔK_1 and ΔL_1) and in surface long-wave feedback (ΔL_1); Their individual contributions are given in Supplementary Fig. 3. The sum of the four component contributions from this offline diagnostic analysis agrees with the model-predicted $\Delta(\lambda E)$ to better than 0.6 W m⁻² (Fig. 2), indicating that nonlinear interactions are negligible among atmospheric forcing, energy allocation and surface feedback. Because this diagnostic analysis is based on the outputs of a single model, the results shown in Fig. 3 do not have error bars (unlike the results presented in Supplementary Fig. 4 for ocean E).

In an effort to understand the surface water temperature adjustment to climate warming, we separate the temporal changes in the temperature difference $\Delta T_s - \Delta T_a$ into two contributions according to the biophysical theory of the surface energy allocation¹⁴,

$$\Delta T_s - \Delta T_a = \frac{\lambda_0}{1 + f} \Delta(R_n^* - G) + \frac{\lambda_0}{(1 + f)^2} \Delta(R_n^* - G) \Delta f \quad (3)$$

where λ_0 is local climate sensitivity, f is a dimensionless energy redistribution factor that is a function of the aerodynamic heat resistance and β , and $R_n^* = (1-a)K_1 + L_1 - \sigma T_a^4$ is apparent net radiation, with σ being the Stefan–Boltzmann constant. According to the theory, variations in the surface

temperature in response to external perturbations are consequences of a local long-wave radiation feedback and energy redistribution between the surface and the overlying atmosphere. Here f was determined with the lake Bowen ratio calculated by the lake simulator and with the heat resistance using a Stanton number of 1.1×10^{-3} for lakes³⁸ and the wind speed at the blending height (~ 50 m) above the surface (u_{50}). According to equation (3), $\Delta T_s - \Delta T_a$ is contributed (1) by changes in the atmospheric forcing variables, surface albedo and heat storage (first term on the right-hand side, labelled AF in Supplementary Fig. 2) and (2) by changes in the energy redistribution factor Δf (second term on the right-hand side, labelled ER in Supplementary Fig. 2). In this analysis, Δf is caused by changes in the lake β , with changes in the aerodynamic resistance omitted due to negligible changes in wind speed ($\Delta u_{50} = 0.06$ m s⁻¹) between the first and last 10 years of the simulation. This attribution analysis reveals that at low latitudes, the slower adjustment of T_s than T_a to climate warming is overwhelmingly associated with the reduction in β and is unrelated to changes in atmospheric forcing (Supplementary Fig. 2b).

CMIP5 data for the oceans. We used outputs from 26 climate models with the RCP 8.5 scenario forcing (2006–2100) from the CMIP5 archive to investigate the global ocean (60°S–60°N) evaporation change (Supplementary Table 2). The surface energy balance variables were analysed using equation (2) to partition the change in ocean E to four component contributions (Supplementary Fig. 4). Variability of the global precipitation temperature sensitivity among the CMIP5 models was interpreted in the framework of the surface energy balance. Specifically, we find that the precipitation temperature sensitivity is highly correlated with the ocean β sensitivity, the surface shortwave radiation sensitivity and the ocean evaporation sensitivity (Fig. 5).

The PT model. We adopted the classic PT model⁹ to help interpret the response of β temperature changes. This model expresses the lake latent heat flux in the open-water season as a proportion to the available energy,

$$\lambda E = \alpha \frac{\Delta}{\Delta + \gamma} (R_n - G) \quad (4)$$

where α is the PT coefficient with a standard value of 1.26, Δ is the slope of the saturated vapour pressure–temperature curve and γ is the psychrometric constant. Combining equation (4) with the Bowen ratio definition and the energy balance equation, we obtain,

$$\beta = \frac{1}{\alpha} \frac{\gamma}{\Delta} + \frac{1}{\alpha} - 1 \quad (5)$$

Because Δ increases exponentially with increasing temperature, this equation predicts that β should decrease with increasing temperature (Fig. 3a) and that the temperature sensitivity of β should be higher in magnitude at lower temperatures (Fig. 3b).

We chose the PT model instead of the Penman–Monteith model because the former allows us to disentangle the effects of radiation and temperature. The theoretical basis of the PT model is the concept of equilibrium evaporation of a wet surface exposed to saturation humidity conditions³⁹. The coefficient α accounts for the fact that in the real atmosphere, the entrainment of dry boundary layer air to the surface layer will cause the actual evaporation to be higher than the equilibrium value. The model has been validated against numerous field experiments^{40–43}. The PT α is bounded by the lower limit of 1.0 and the upper limit of about 1.6 (ref. 9). At the lower limit, evaporation occurs at the equilibrium rate when the surface air is at saturation; at the upper limit, all of the available energy is consumed by evaporation and no sensible heat flux to the atmosphere is allowed. Our lake modelling results suggest that the optimal PT α for lakes is 1.31, which is higher than the original value of 1.26 (Fig. 3). This higher α values also describes the energy partitioning of the global oceans according to observational data¹⁵ and the mean behaviour of ocean E in the CMIP5 models under current climate conditions (Supplementary Fig. 5).

Code availability. The code used to generate the global lake evaporation result can be accessed at https://svn-ccsm-models.cgd.ucar.edu/clm2/release_tags/cesm1_2_x_n15_clm4_5_10/models/Ind/clm/src/clm4_5/ (user name: guest user; password: friendly). The CLM4.5 code is part of CESM.

Data availability. The data that support the findings of this study are available from the corresponding author upon request and are also available on the unstructured repository of figshare at <https://figshare.com/s/d7f75ce7ec482e64fde7>. The CMIP5 data are available from the Earth System Grid Federation (ESGF) Portal at <https://esgf-node.llnl.gov/search/cmip5>.


References

- Henderson-Sellers, B. New formulation of eddy diffusion thermocline models. *Appl. Math. Model.* **9**, 441–446 (1985).

32. Hostetler, S. W. & Bartlein, P. J. Simulation of lake evaporation with application to modeling lake level variations of Harney-Malheur Lake, Oregon. *Water Resour. Res.* **26**, 2603–2612 (1990).
33. Fang, X. & Stefan, H. G. Long-term lake water temperature and ice cover simulations/measurements. *Cold Reg. Sci. Technol.* **24**, 289–304 (1996).
34. Lawrence, D. M. et al. Parameterization improvements and functional and structural advances in Version 4 of the Community Land Model. *J. Adv. Model. Earth Syst.* **3**, M03001 (2011).
35. Zhao, L., Lee, X. & Schultz, N. M. A wedge strategy for mitigation of urban warming in future climate scenarios. *Atmos. Chem. Phys.* **17**, 9067–9080 (2017).
36. Richter, I. & Xie, S.-P. Muted precipitation increase in global warming simulations: a surface evaporation perspective. *J. Geophys. Res.* **113**, D24118 (2008).
37. Peel, M. C., Finlayson, B. L. & McMahon, T. A. Updated world map of the Köppen-Geiger climate classification. *Hydrol. Earth Syst. Sci.* **11**, 1633–1644 (2007).
38. Xiao, W. et al. Transfer coefficients of momentum, heat and water vapour in the atmospheric surface layer of a large freshwater lake. *Bound. Lay. Meteorol.* **148**, 479–494 (2013).
39. de Bruins, H. A. R. A model for the Priestley-Taylor parameter alpha. *J. Clim. Appl. Meteorol.* **22**, 572–578 (1983).
40. dos Reis, R. J. & Dias, N. L. Multi-season lake evaporation: energy-budget estimates and CRLE model assessment with limited meteorological observations. *J. Hydrol.* **208**, 135–147 (1998).
41. Elsawwaf, M., Willems, P. & Feyen, J. Assessment of the sensitivity and prediction uncertainty of evaporation models applied to Nasser Lake, Egypt. *J. Hydrol.* **395**, 10–22 (2010).
42. Gallego-Elvira, B., Baille, A., Martín-Gorrioz, B. & Martínez-Alvarez, V. Energy balance and evaporation loss of an agricultural reservoir in a semi-arid climate (south-eastern Spain). *Hydrol. Process.* **24**, 758–766 (2010).
43. Lee, X. et al. The Taihu Eddy Flux Network: an observational program on energy, water, and greenhouse gas fluxes of a large freshwater lake. *Bull. Am. Meteorol. Soc.* **95**, 1583–1594 (2014).

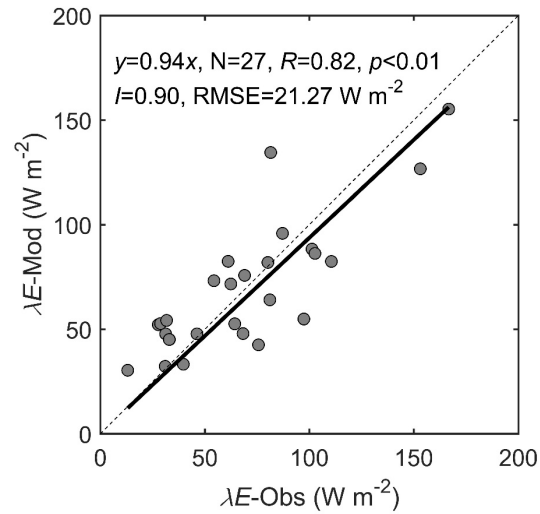
In the format provided by the authors and unedited.

Global lake evaporation accelerated by changes in surface energy allocation in a warmer climate

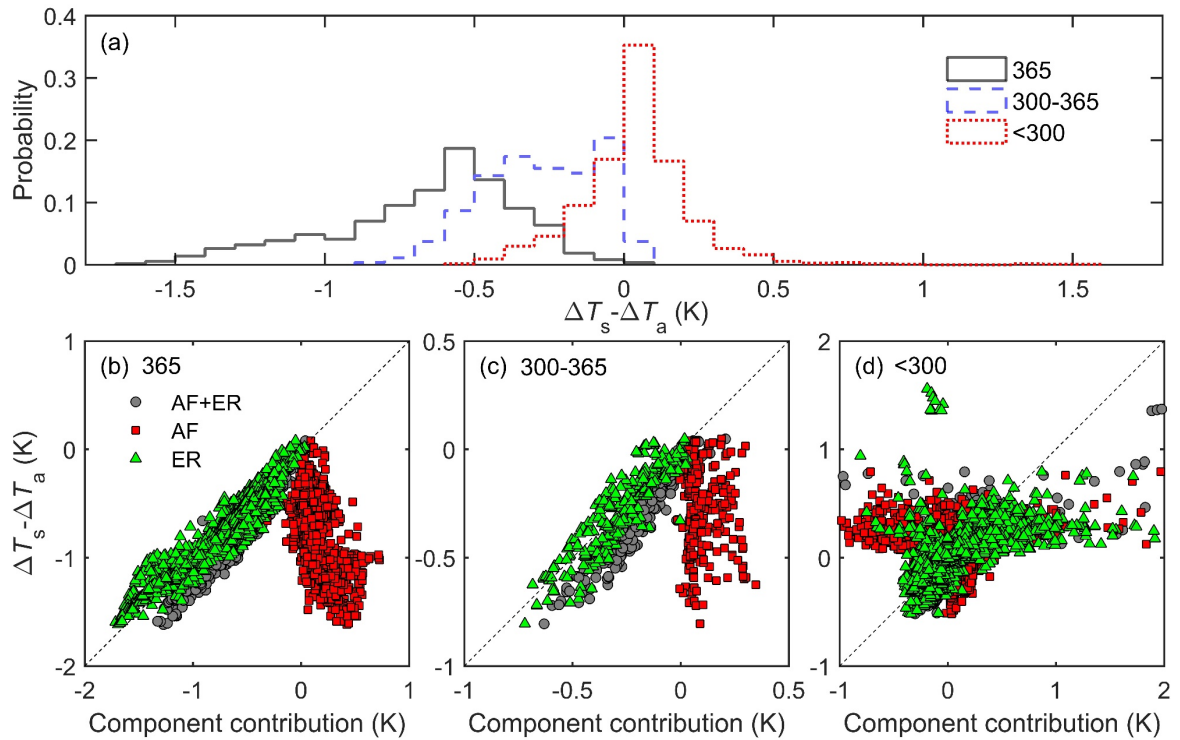
Wei Wang ^{1,2,5}, Xuhui Lee^{1,3*}, Wei Xiao ^{1,2,5}, Shoudong Liu ^{1,2}, Natalie Schultz ³, Yongwei Wang^{1,2},
Mi Zhang ^{1,2} and Lei Zhao ^{1,4}

¹Yale-NUIST Center on Atmospheric Environment, International Joint Laboratory on Climate and Environment Change, Nanjing University of Information Science & Technology, Nanjing, China. ²Key Laboratory of Meteorological Disaster, Ministry of Education & Collaborative Innovation Center on Forecast and Evaluation of Meteorological Disasters, Nanjing University of Information Science & Technology, Nanjing, China. ³School of Forestry and Environmental Studies, Yale University, New Haven, CT, USA. ⁴Program in Science, Technology, and Environmental Policy, Woodrow Wilson School of Public and International Affairs, Princeton University, Princeton, NJ, USA. ⁵These authors contributed equally: Wei Wang and Wei Xiao. *e-mail: xuhui.lee@yale.edu

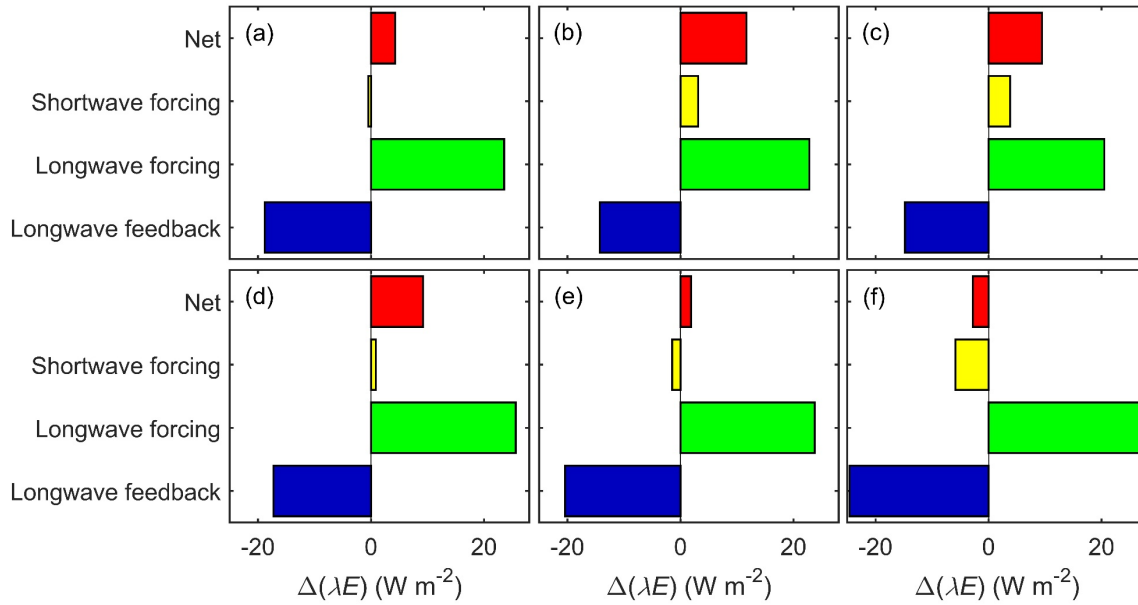
Supplementary Figure 1: Comparison of lake latent heat flux. Each data point represents a comparison of the latent heat flux calculated by the model (λE -Mod) against the observed annual mean latent heat flux found in the literature (λE -Obs). Solid line represents linear regression through the origin with regression statistics noted (N : number of observations; R , linear correlation coefficient; p , significance level; I , index of agreement; RMSE, root-mean-square error)



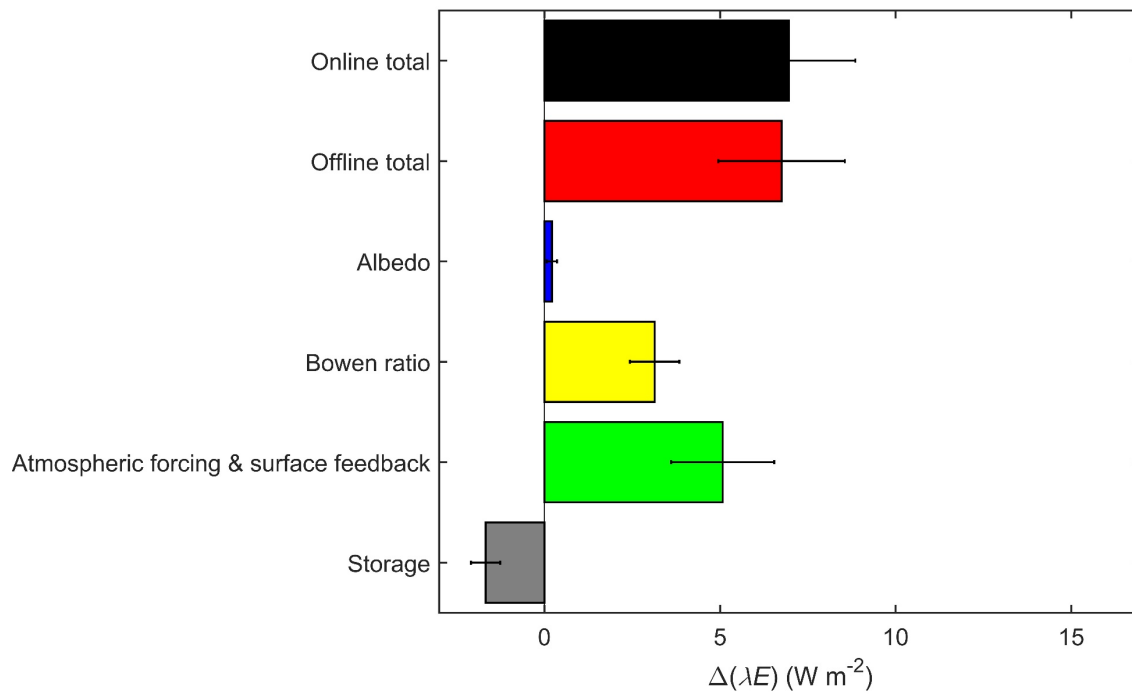
Supplementary Figure 2: Adjustment of lake surface temperature to climate warming. (a) Histograms of lake-air temperature gradient change ($\Delta T_s - \Delta T_a$) (2091 – 2100 mean minus 2006 – 2015 mean) for lakes with different open-water periods: black solid line, current annual open water days equal to 365; blue dashed line: current annual open water days between 300 and 365; red dotted line: current annual open water days fewer than 300. (b), (c), (d): Partitioning of lake-air temperature gradient change into two components for the three groups of lakes shown in (a): atmospheric forcing and heat storage (AF) and energy redistribution (ER)



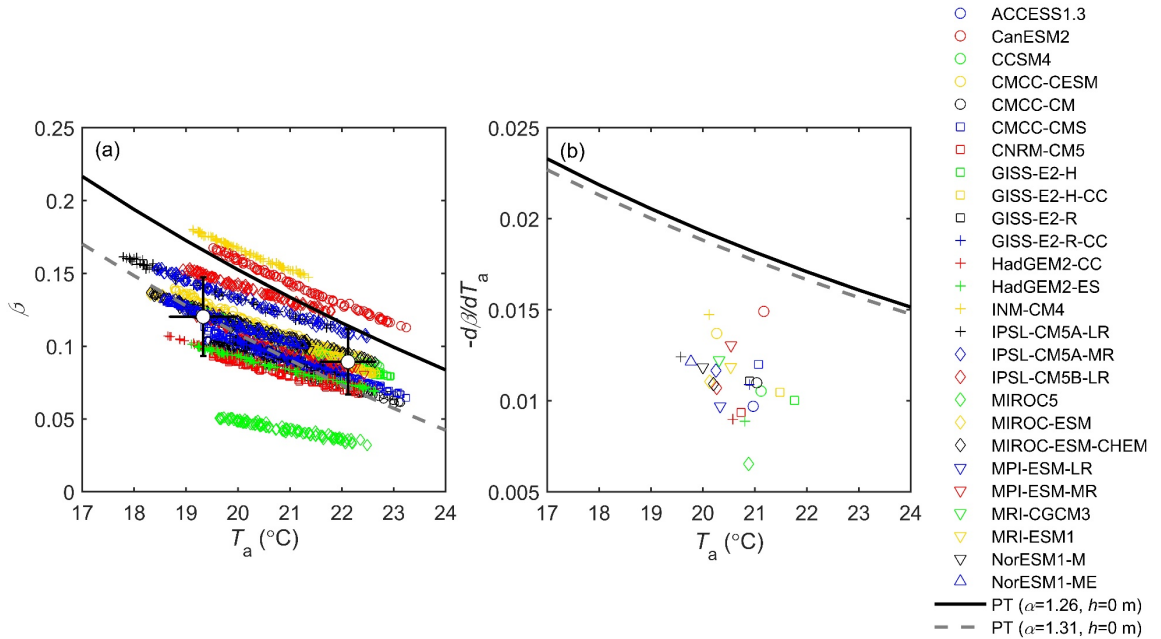
Supplementary Figure 3: Atmospheric forcing versus surface feedback. (a) global; (b) tropical; (c) temperate; (d) arid; (e) cold; (f) polar. Yellow, green and blue bars are component contributions of atmospheric forcing (yellow and green) and surface feedback (blue) to the lake latent heat flux change, and red bars are net contributions.



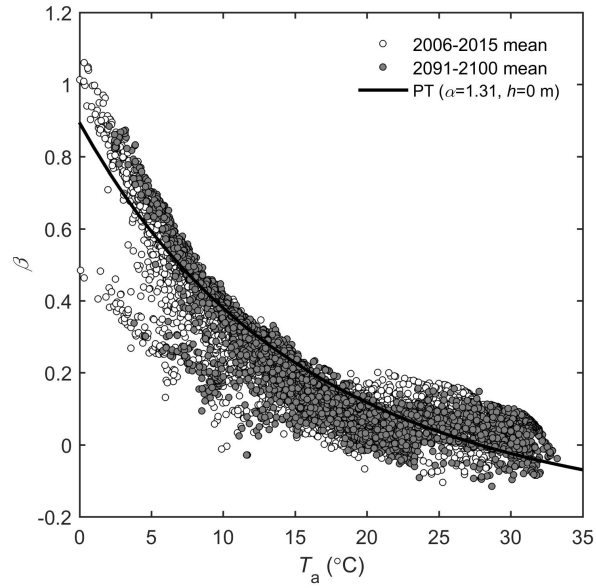
Supplementary Figure 4: Attribution of ocean latent heat flux. Black bars – $\Delta(\lambda E)$ (2091 – 2100 mean minus 2006 – 2015 mean) predicted by 26 CMIP5 models; red bars – calculated as the sum of the four component contributions, blue bars – contribution by albedo change, yellow bars – contribution by Bowen ratio change, green bars – contributions by changes in atmospheric forcing and surface feedback, grey bars – contribution by change in heat storage. Error bars are ± 1 standard deviation of 26 CMIP5 models



Supplementary Figure 5: Temperature controls on ocean Bowen ratio. (a) Annual mean Bowen ratio (β) varying with annual mean air temperature (T_a) for CMIP5 26 models. The means of the 26 models for the first 10 years and the last 10 years are shown as white filled circles with error bars indicating ± 1 standard deviation. (b) Bowen ratio temperature sensitivity for the 26 models. The Priestley-Taylor (PT) model prediction is shown as a solid line ($\alpha = 1.26$) and a dashed line ($\alpha = 1.31$) at sea level ($h = 0$ m)



Supplementary Figure 6: Temperature controls on lake Bowen ratio for two periods. Open circles are mean values of the first 10 years (2006-2015) and filled circles are mean values of the last 10 years (2091-2100) of the model simulation. Each data point represents one lake. The solid line is the Priestley-Taylor (PT) model prediction with $\alpha = 1.31$ and elevation $h = 0$ m.



Supplementary Table 1. A list of lake evaporation data found in the published literature. Each observation is the mean of open water period for at least one year.

Inland water bodies	Location	h	A	d_{mean}	d_{max}	Method	Period	T_a	H	λE	β	Reference
Emaiksoun Lake	71.23° N, 156.23° W	8	1.857	1.847	2.56	BREB	2008-2010	4.5	26.2	34.5	0.759	Potter, 2011
Great Bear Lake	65.80° N, 120.80° W	156	31000	72	413	EC	2004-2005	1.3	10.5	13.1	0.806	Rouse et al., 2008
Skeeter Lake	63.58° N, 113.88° W	339	0.047	3.2	6.6	BREB	1999-2000	12.0	22.0	75.7	0.291	Spence et al., 2003
Sleepy Dragon Lake	62.92° N, 112.92° W	330	5.46	12	35	BREB	2000-2002	12.6	15.7	68.2	0.230	Rouse et al., 2005
Gar Lake	62.52° N, 114.37° W	186	0.296	0.5	0.9	BREB	2000-2002	12.8	37.8	64.3	0.588	Rouse et al., 2005
Great Slave Lake	61.60° N, 114.00° W	160	27000	41	614	EC	1997-2002	2.7	28.3	46.2	0.613	Rouse et al., 2008
Lake Valkea-Kotinen	61.23° N, 25.05° E	156	0.041	2.5	6.5	EC	2005-2008	10.5	17.6	31.2	0.564	Nordbo et al., 2011
Großer Kossenblatter See	52.13° N, 14.10° E	43	1.68	2	5	EC	05/2003-11/2003	16.0	8.0	69.0	0.116	Beyrich et al., 2006
Lake Superior	47.18° N, 88.28° W	183	82100	148	406	EC	06/2008-11/2010	9.8	11.9	27.7	0.427	Blanken et al., 2011
Lake Williams	47.13° N, 99.60° W	423	0.36	5.2	9.8	BREB	1982-1986	12.5	16.3	73.7	0.221	Sturrock et al., 1992
Lake Sparkling	46.02° N, 89.70° W	494	0.64	10.9	20	BREB	1989-1998	14.8	19.9	97.4	0.204	Lenters et al., 2005
Lake Huron	44.67° N, 82.28° W	176	59570	53	228	BT	1992-1997	9.8	13.6	28.8	0.473	Lofgren et al., 2000
Lake Michigan	43.90° N, 86.23° W	177	58016	84	281	BT	1992-1996	12.1	11.0	32.9	0.333	Lofgren et al., 2000
Lake Ontario	43.70° N, 78.03° W	75	19009	86	224	BT	1992-1999	12.7	9.7	31.7	0.307	Lofgren et al., 2000
Mirror Lake	43.62° N, 71.26° W	213	0.15	5.75	11	BREB	1982-1987	14.1	18.4	67.9	0.272	Rosenberry et al., 2007
Thau Lagoon	43.40° N, 3.60° E	-2	75	4	11	BT, EC	2008-2010	14.9	5.4	81.1	0.066	Bouin et al., 2012
Lake Mendota	43.01° N, 89.42° W	850	39.4	12.2	25	BREB	1958-1959	12.1	22.0	85.9	0.257	Dutton & Bryson, 1959

American Falls Reservoir	42.80° N, 112.70° W	1330	227	9	16.15	BREB, EC	05-11/2004	12.0	18.1	61.1	0.297	Allen & Tasumi, 2005
Lake Erie	42.20° N, 81.20° W	174	25821	17.7	64	BT	1992-1998	13.4	11.9	54.3	0.219	Lofgren et al., 2000
Mar Menor Lagoon	37.72° N, 0.83° W	-1	135.5	4.5	7	BT	2003-2006	16.0	19.7	101.3	0.194	Martinez-Alvarez et al., 2011
Spain agricultural water reservoir	37.58° N, 0.98° W	0	0.0024	5	5	BT	2007	17.8	10.6	102.7	0.103	Gallego-Elvira et al., 2010
Ross Barnett Reservoir	32.43° N, 90.03° W	118	130	5	8	EC	2008	17.7	17.1	87.1	0.196	Liu et al., 2012
Lake Taihu	31.40° N, 120.22° E	1	2338	1.9	2.6	EC	06/2010-now	16.6	10.7	80.1	0.134	Wang et al., 2014
Lake Ikeda	31.23° N, 130.92° E	88	10.62	125	233	NM	1981-2005	17.9	14.0	72.0	0.194	Momii and Ito, 2008
Nam Co	30.77° N, 90.99° E	4718	1980	33	125	BREB	2006-2008	2.3	25.3	62.4	0.405	Haginoya et al., 2009
Yamdruk Yumco	28.93° N, 90.68° E	4442	638	23.6	59	BT	1961-2005	4.7	22.3	110.6	0.202	Yu et al., 2011
Indian pond	25.60° N, 75.25° E	252	0.0047	2.75	3	BREB	2002-2005	23.3	5.7	81.5	0.070	Ali et al., 2008
Lake Nasser	22.98° N, 32.12° E	183	5248	25.2	130	BREB, BT	1995-2004	27.2	-6.7	166.7	-0.040	Elsawwaf and Willems, 2012
Lake Valencia	10.00° N, 67.00° E	410	350	19	39	BREB	1977-1978	26.3	20.8	149.3	0.140	Lewis Jr, 1983
Lake Ziway	7.90° N, 38.75° E	1636	490	2.5	9	BREB	1969-1990	19.9	20.7	137.7	0.150	Vallet-Coulomb et al., 2001
Lake Victoria	1.00° S, 33.00° E	1134	68800	40	84	BREB	1956-1978	22.3	15.5	118.5	0.131	Yin & Nicholson, 1998
Lake Tanganyika	3-9° S, 29-31° E	775	32600	570	1470	BT	1993-1996	25.3	8.7	153.1	0.057	Verburg & Antenucci, 2010
Lake Titicaca	15.62° S, 69.57° W	3812	8372	107	281	BREB, BT, WB	1964-1978	8.2	28.9	135.0	0.214	Delclaux et al., 2007
Logan's Dam	27.57° S, 152.34° E	88	0.168	4.3	6	LAS	11/2009-05/2011	20.6	7.9	98.2	0.080	McJannet et al., 2013

Note 1: Symbols and abbreviations: h – lake elevation above sea level (m); A – surface area (km^2); d_{mean} – mean depth (m); d_{max} – maximum

depth (m); T_a – mean surface air temperature ($^{\circ}\text{C}$); H – sensible heat flux (W m^{-2}); λE – latent heat flux (W m^{-2}); β – Bowen ratio; EC – eddy

covariance; BT – bulk transfer algorithm; BREB – Bowen ratio energy balance; NM – numerical modeling based on the Priestley-Taylor formula; WB – water budget method; LAS – large aperture scintillometer.

Note 1: Of the 34 inland water bodies listed, 27 are resolved by the CLM4.5 at the subscript level and are used for comparison shown in Extended Data Figure 1.

Supplementary Table 2. Description on the 26 CMIP5 models used in the study

Model name	Modeling center or group	Institute ID	Horizontal resolution (grid numbers: longitude×latitude)
ACCESS1.3	Commonwealth Scientific and Industrial Research Organization (CSIRO) and Bureau of Meteorology (BOM), Australia	CSIRO-BOM	192×145
CanESM2	Canadian Centre for Climate Modelling and Analysis	CCCMA	128×64
CCSM4	National Center for Atmospheric Research	NCAR	288×192
CMCC-CESM	Centro Euro-Mediterraneo per I Cambiamenti Climatici	CMCC	96×48
CMCC-CM			480×240
CMCC-CMS			192×96
CNRM-CM5	Centre National de Recherches Météorologiques / Centre Européen de Recherche et Formation Avancée en Calcul Scientifique	CNRM-CERFACS	256×128
GISS-E2-H	NASA Goddard Institute for Space Studies	NASA GISS	144×90
GISS-E2-H-CC			144×90
GISS-E2-R			144×90
GISS-E2-R-CC			144×90
HadGEM2-CC	Met Office Hadley Centre (additional HadGEM2-ES realizations contributed by Instituto Nacional de Pesquisas Espaciais)	MOHC (additional realizations by INPE)	192×145
HadGEM2-ES			192×145
INM-CM4	Institute for Numerical Mathematics	INM	180×120

IPSL-CM5A-LR	Institut Pierre-Simon Laplace	IPSL	96×96
IPSL-CM5A-MR			144×143
IPSL-CM5B-LR			96×96
MIROC5	Atmosphere and Ocean Research Institute (The University of Tokyo), National Institute for Environmental Studies, and Japan Agency for Marine-Earth Science and Technology	MIROC	256×128
MIROC-ESM	Japan Agency for Marine-Earth Science and Technology, Atmosphere and Ocean Research Institute (The University of Tokyo), and National Institute for Environmental Studies	MIROC	128×64
MIROC-ESM-CHEM			128×64
MPI-ESM-LR	Max-Planck-Institut für Meteorologie (Max Planck Institute for Meteorology)	MPI-M	192×96
MPI-ESM-MR			192×96
MRI-CGCM3	Meteorological Research Institute	MRI	320×160
MRI-ESM1			320×160
NorESM1-M	Norwegian Climate Centre	NCC	144×96
NorESM1-ME			144×96

Reference

- Ali, S., Ghosh, N. C. & Singh, R. Evaluating best evaporation estimate model for water surface evaporation in semi-arid region, India. *Hydrological Process* **22**, 1093-1106, doi:10.1002/hyp.6664 (2008).
- Allen, R. G. & Tasumi, M. Evaporation from American Falls Reservoir in Idaho via a Combination of Bowen Ratio and Eddy Covariance. *ASCE*, 2005.
- Beyrich, F. et al. Area-averaged surface fluxes over the litfass region based on eddy-covariance measurements. *Bound-Lay Meteorol* **121**, 33-65, doi:DOI 10.1007/s10546-006-9052-x (2006).
- Blanken, P. D., Spence, C., Hedstrom, N. & Lenters, J. D. Evaporation from Lake Superior: 1. Physical controls and processes. *J Great Lakes Res* **37**, 707-716, doi:DOI 10.1016/j.jglr.2011.08.009 (2011).
- Bouin, M.-N., Caniaux, G., Traullé, O., Legain, D. & Le Moigne, P. Long-term heat exchanges over a Mediterranean lagoon. *Journal of Geophysical Research: Atmospheres* **117**, D23104, doi:10.1029/2012jd017857 (2012).
- Delclaux, F., Coudrain, A. & Condom, T. Evaporation estimation on Lake Titicaca: a synthesis review and modelling. *Hydrol Process* **21**, 1664-1677, doi:Doi 10.1002/Hyp.6360 (2007).
- Dutton, J. A. & Bryson, R. A. HEAT FLUX IN LAKE MENDOTA1. *Limnology and Oceanography* **7**, 80-97, doi:10.4319/lo.1962.7.1.0080 (1962).
- Elsawwaf, M. & Willems, P. Analysis of the climate variability on Lake Nasser evaporation based on the Bowen ratio energy budget method. *J Environ Biol* **33**, 475-485 (2012).
- Gallego-Elvira, B., Baille, A., Martin-Gorriz, B. & Martinez-Alvarez, V. Energy balance and evaporation loss of an agricultural reservoir in a semi-arid climate (south-eastern Spain). *Hydrol Process* **24**, 758-766, doi:Doi 10.1002/Hyp.7520 (2010).
- Haginoya, S. et al. Air–Lake Interaction Features Found in Heat and Water Exchanges over Nam Co on the Tibetan Plateau. *SOLA* **5**, 172-175 (2009).
- Lenters, J. D., Kratz, T. K. & Bowser, C. J. Effects of climate variability on lake evaporation: Results from a long-term energy budget study of Sparkling Lake, northern Wisconsin (USA). *J Hydrol* **308**, 168-195, doi:DOI 10.1016/j.jhydrol.2004.10.028 (2005).
- Lewis, W. M. Temperature, heat, and mixing in Lake Valencia, Venezuela1. *Limnology and Oceanography* **28**, 273-286, doi:10.4319/lo.1983.28.2.0273 (1983).
- Liu, H. P., Zhang, Q. Y. & Dowler, G. Environmental Controls on the Surface Energy Budget over a Large Southern Inland Water in the United States: An Analysis of One-Year Eddy Covariance Flux Data. *J Hydrometeorol* **13**, 1893-1910, doi:Doi 10.1175/Jhm-D-12-020.1 (2012).

- Lofgren, B. M. & Zhu, Y. C. Surface energy fluxes on the Great Lakes based on satellite-observed surface temperatures 1992 to 1995. *J Great Lakes Res* **26**, 305-314 (2000).
- Martinez-Alvarez, V., Gallego-Elvira, B., Maestre-Valero, J. F. & Tanguy, M. Simultaneous solution for water, heat and salt balances in a Mediterranean coastal lagoon (Mar Menor, Spain). *Estuar Coast Shelf S* **91**, 250-261, doi:DOI 10.1016/j.ecss.2010.10.030 (2011).
- McJannet, D. et al. Long-term energy flux measurements over an irrigation water storage using scintillometry. *Agricultural and Forest Meteorology* **168**, 93-107, doi:http://dx.doi.org/10.1016/j.agrformet.2012.08.013 (2013).
- Momii, K. & Ito, Y. Heat budget estimates for Lake Ikeda, Japan. *J Hydrol* **361**, 362-370, doi:DOI 10.1016/j.jhydrol.2008.08.004 (2008).
- Nordbo, A. et al. Long-term energy flux measurements and energy balance over a small boreal lake using eddy covariance technique. *J Geophys Res-Atmos* **116**, doi:Artn D02119 Doi 10.1029/2010jd014542 (2011).
- Potter, B. Climatic controls on the summertime energy balance of a thermokarst lake in northern Alaska: short-term, seasonal, and interannual variability. Dissertations & Theses in Natural Resources. Paper 39, University of Nebraska-Lincoln (2011).
- Rosenberry, D. O., Winter, T. C., Buso, D. C. & Likens, G. E. Comparison of 15 evaporation methods applied to a small mountain lake in the northeastern USA. *J Hydrol* **340**, 149-166, doi:DOI 10.1016/j.jhydrol.2007.03.018 (2007).
- Rouse, W. R. et al. The role of northern lakes in a regional energy balance. *J Hydrometeorol* **6**, 291-305 (2005).
- Rouse, W. R. et al. Investigation of the Thermal and Energy Balance Regimes of Great Slave and Great Bear Lakes. *J Hydrometeorol* **9**, 1318-1333, doi:Doi 10.1175/2008jhm977.1 (2008).
- Spence, C., Rouse, W. R., Worth, D. & Oswald, C. Energy budget processes of a small northern lake. *J Hydrometeorol* **4**, 694-701 (2003).
- Sturrock, A. M., Winter, T. C. & Rosenberry, D. O. Energy Budget Evaporation from Williams Lake - a Closed Lake in North Central Minnesota. *Water Resour Res* **28**, 1605-1617 (1992).
- Vallet-Coulomb, C., Legesse, D., Gasse, F., Travi, Y. & Chernet, T. Lake evaporation estimates in tropical Africa (Lake Ziway, Ethiopia). *J Hydrol* **245**, 1-18 (2001).
- Verburg, P. & Antenucci, J. P. Persistent unstable atmospheric boundary layer enhances sensible and latent heat loss in a tropical great lake: Lake Tanganyika. *J Geophys Res-Atmos* **115**, doi:Artn D11109 Doi 10.1029/2009jd012839 (2010).

Wang, W. et al. Temporal and spatial variations in radiation and energy balance across a large freshwater lake in China. *Journal of Hydrology* **511**, 811-824, doi:<http://dx.doi.org/10.1016/j.jhydrol.2014.02.012> (2014).

Yin, X. G. & Nicholson, S. E. The water balance of Lake Victoria. *Hydrolog Sci J* **43**, 789-811 (1998).

Yu, S. M., Liu, J. S., Xu, J. Q. & Wang, H. Evaporation and energy balance estimates over a large inland lake in the Tibet-Himalaya. *Environ Earth Sci* **64**, 1169-1176, doi:DOI 10.1007/s12665-011-0933-z (2011).